



HAL
open science

Unravelling the last milliseconds of an individual graphene nanoplatelet before impact with a Pt surface by bipolar electrochemistry

Zejun Deng, Christophe Renault

► **To cite this version:**

Zejun Deng, Christophe Renault. Unravelling the last milliseconds of an individual graphene nanoplatelet before impact with a Pt surface by bipolar electrochemistry. *Chemical Science*, 2021, 12 (37), pp.12494-12500. 10.1039/D1SC03646G . hal-03437450

HAL Id: hal-03437450

<https://hal.science/hal-03437450>

Submitted on 19 Nov 2021

HAL is a multi-disciplinary open access archive for the deposit and dissemination of scientific research documents, whether they are published or not. The documents may come from teaching and research institutions in France or abroad, or from public or private research centers.

L'archive ouverte pluridisciplinaire **HAL**, est destinée au dépôt et à la diffusion de documents scientifiques de niveau recherche, publiés ou non, émanant des établissements d'enseignement et de recherche français ou étrangers, des laboratoires publics ou privés.

1 Contact-less Monitoring of Dynamics and Reactivity 2 of Individual Graphene Nanoplatelets from μm to 3 nm from an Electrified Interface

4 *Zejun Deng*^{1,†}, and *Christophe Renault*^{1,*}

5 ¹Laboratoire de Physique de la Matière Condensée, Ecole Polytechnique, CNRS, IP Paris,
6 Route de Saclay, 91128, Palaiseau, France

7 KEYWORDS. Contact-less interactions, Near-surface dynamics, Graphene Nanoplatelet,
8 Bipolar Electrochemistry, Single Entity Electrochemistry, Correlated opto-electrochemical
9 measurement

10 ABSTRACT: Contact-less interactions of micro/nano-particles near electrochemically or
11 chemically active interfaces are ubiquitous in chemistry and biochemistry. Forces arising from a
12 convective field, an electric field or chemical gradients act on different scales ranging from few
13 microns down to few nanometers making their study difficult. Here, we correlated optical
14 microscopy and electrochemical measurements to track at the millisecond timescale the
15 dynamics of individual 2D particles, Graphene Nanoplatelet (GNP), when approaching an
16 electrified Pt micro-interface. Our original approach takes advantage of the bipolar feedback
17 current recorded when a conducting particle approaches an electrified surface without electrical
18 contact and numerical simulations to access the velocity of individual GNPs. We evidenced a

1 strong deceleration of GNPs from few tens of $\mu\text{m/s}$ down to few $\mu\text{m/s}$ within the last μm above
2 the surface. This observation reveals the existence of strongly non-uniform forces between tens
3 of and a thousand nanometers from the surface.

4 **Introduction**

5 Interaction between particles and surfaces is ubiquitous in biology and chemistry.¹⁻⁴ Forces
6 controlling the approach of a single platelet from a blood vessel or a single active metal
7 nanoparticle from an electrode control strongly the efficiency of the interaction and thus need to
8 be precisely understood.^{5, 6} Observation of both close- and long-range forces on individual
9 particles with dynamics of few ms is an extraordinarily challenging task. Single entity
10 electrochemistry proved to be a powerful method to study individual nanoparticles.⁷⁻¹² The high
11 temporal resolution of electrochemical measurements allows probing dynamics of electro-
12 catalysis,¹³⁻¹⁷ electrolysis,¹⁸⁻²³ electro-nucleation and growth,²⁴⁻³⁰ as well as motion of individual
13 particles.³¹⁻³⁵ For example, several groups showed that Ag nanoparticles (Ag NP) may rebound
14 several times on the surface of the electrode before being completely oxidized.^{20, 21, 23} White and
15 coworkers showed that the dynamics of the rebound controls the overall kinetic of Ag NP
16 oxidation and can be tuned by adjusting the viscosity of the solution.³⁶ These works revealed the
17 potential complexity of nanoparticle dynamics near a surface.

18 Uncovering the complexity of nanoparticle dynamics often necessitates the combination of
19 electrochemistry with optical techniques. Among the different optical techniques used so far are
20 3D super-resolution holography,¹⁸ surface plasmonic resonance microscopy,^{37, 38} backside
21 absorbing layer microscopy (BALM),³² fluorescent microscopy,¹⁹ dark-field microscopy,^{39, 40}
22 and many others.^{12, 41} For example, Tschulik and coworkers combined dark-field microscopy and
23 hyperspectral imaging with electrochemistry to study the oxidation of single Ag NP in the

1 presence of Cl^- .³⁹ They observed that the intensity decrease of the optical signal is caused by the
2 reversible formation of AgCl rather than by Ag dissolution. Kanoufi and coworkers utilized
3 BALM to image the reduction dynamics of single silver halide NP and visualized that the NP
4 conversion proceeds to completion through the formation of multiple inclusions rather than by
5 the classical core-shrinking mechanism.³²

6 Recently, Thorgaard and Lemay's groups observed complex toroidal trajectories of
7 fluorescent particles revealing electro-osmotic flow near an ultra-microelectrode (UME) under
8 supporting electrolyte of low concentrations.^{33, 34} We also showed that two-dimensional (2D)
9 graphene nanoplatelets (GNPs) collide on the surface of a UME with a preferential up-right
10 orientation and then, rotate at few °/ms to lay flat on the electrode surface.³⁵ Up to now
11 monitoring dynamics of individual nanoparticles by single entity electrochemistry required
12 electrical contact and thus could only provide indirect information on particle motion when this
13 latter is not in contact with the surface of the electrode.

14 In this article, we combined time-resolved bright-field microscopy and electrochemistry
15 with finite element simulation to investigate in a contact-less mode the motion of individual
16 GNPs at few μm above the surface of a UME. The contact-less tracking of GNPs is based on a
17 novel concept of transient bipolar feedback. We investigated the effect of viscosity on the
18 velocity of GNP approaching the UME and determined velocity profiles of single GNPs with a
19 time resolution of ms and spanning from a couple of microns to solely few tens of nanometers
20 away from the surface of a Pt micro-interface.

21 **Results and Discussion**

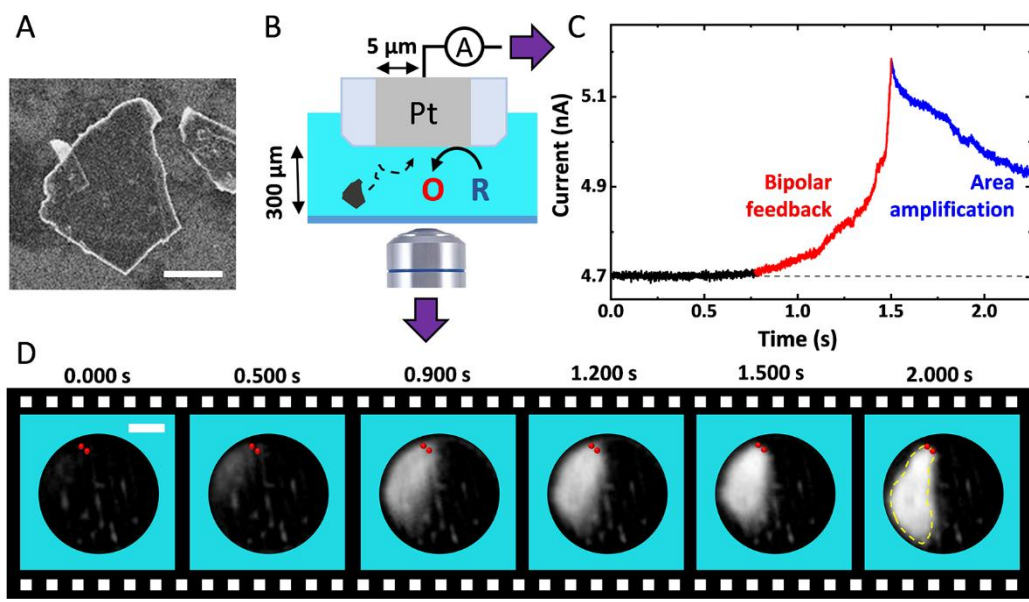
22

23 Figure 1A shows a typical GNP c.a. 15 nm thick and $3.2 \pm 2.0 \mu\text{m}$ long (see Figure S3).

1 Figure 1B shows the experimental setup used to monitor the approach of individual GNPs toward
2 the surface of the Pt UME. The UME is facing downward with its surface positioned 300 μm
3 above a coverslip closing the bottom of the opto-electrochemical cell. A two-electrode setup is
4 used to apply a potential and measure the current. The Pt UME is biased at 0.4 V to drive mass-
5 transfer limited oxidation of 1,1'-ferrocenedimethanol (FcDM). The camera and the ammeter are
6 synchronized externally and data is collected at 1 kHz and 2 kHz, respectively (see Figure S5).

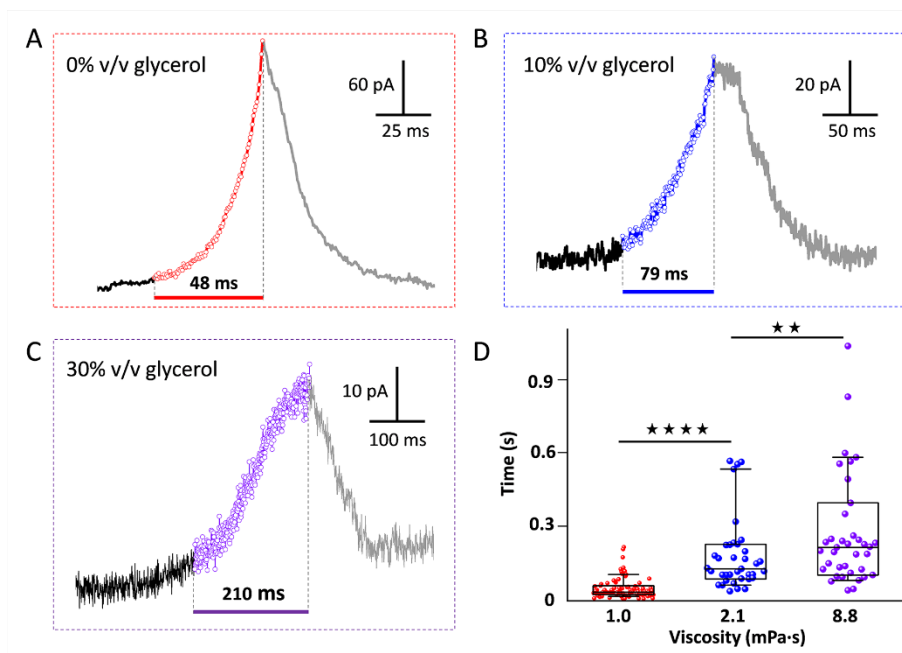
7 Figure 1C shows a typical chronoamperogram starting with a steady-state current of 4.702 nA
8 corresponding to the oxidation of FcDM on Pt. At 0.772 s the current rises to 5.183 nA (red
9 trace). The rise is followed by decay after 1.500 s. Such current transients are never observed in
10 absence of GNP (see Figure S6).

11 Figure 1D shows simultaneous optical micrographs of the Pt disk, and the full movie is provided
12 in Movie S1. The Pt disk looks dark while the GNP looks bright. At 0.500 s a white shadow
13 appears on the top left side of the micrographs. Progressively the edges of an individual GNP can
14 be distinguished. At 2.000 s the GNP lays down on the Pt surface and does not move anymore
15 allowing to capture a sharp image of the edges of the GNP (the contour of the GNP is
16 highlighted by the yellow dashed line). The red points on all the micrographs were incrustated to
17 evidence that the top side of the GNP appears sharp and does not move anymore after c.a. 1.500
18 s. At that time the top edge of the GNP is touching the Pt surface while the rest of the GNP is
19 still in solution, out of focus. We recently explained how the rotation of a GNP, once in contact
20 with the UME, can lead via area amplification to current decays such as the one observed after
21 2.000 s (blue portion of the curve shown in Figure 1C).³⁵ However, a far more surprising
22 observation here is the increase of current *before* the GNP enters in contact with the UME.



1
 2 Figure 1. (A) SEM image of a GNP adsorbed on a Si substrate. The scale bar represents 1 μm. (B) Scheme of
 3 the opto-electrochemical cell used to simultaneously record a video of the surface of a 5 μm radius Pt UME
 4 and the current passing through this latter. O and R represent FcDM⁺ and FcDM, respectively. (C)
 5 Chronoamperogram recorded at 2 kHz with the Pt UME biased at 0.4 V vs Ag/AgCl 3.4M KCl in presence of
 6 3.5 mM FcDM, 0.01% v/v PSS and 0.43 mg/mL GNP. (D) Bright-field optical micrographs of the Pt surface
 7 recorded in synchronization with the chronoamperogram in (C). The red points and yellow dashed lines are
 8 manually drawn to indicate the position where the GNP first touches the Pt surface and then the edges of the
 9 GNP, respectively. The simultaneous movie and current trace are provided in Movie S1.

10 Figure 2(A-C) show representative current spikes recorded for different GNP suspensions
 11 having different viscosity. The viscosity was varied from 1.0 to 8.8 mPa·s by the addition of
 12 glycerol (see Figure S7). Figure 2D shows the average rise time of the current spike as a
 13 function of the viscosity of the solution. Higher viscosity leads to a longer current rise time.
 14 Since the motion of the GNP is directly affected by the viscosity of the solution, we conclude
 15 that the rise of the current transient and the motion of the GNP are correlated.



1
 2 Figure 2. Representative current transients in the presence of (A) 0, (B) 10 and (C) 30% v/v
 3 glycerol, with a viscosity of 1.0, 2.1 and 8.8 mPa·s, respectively. (D) Statistical analysis of the
 4 average duration of the current rise. (**p < 0.01, ****p < 0.0001).

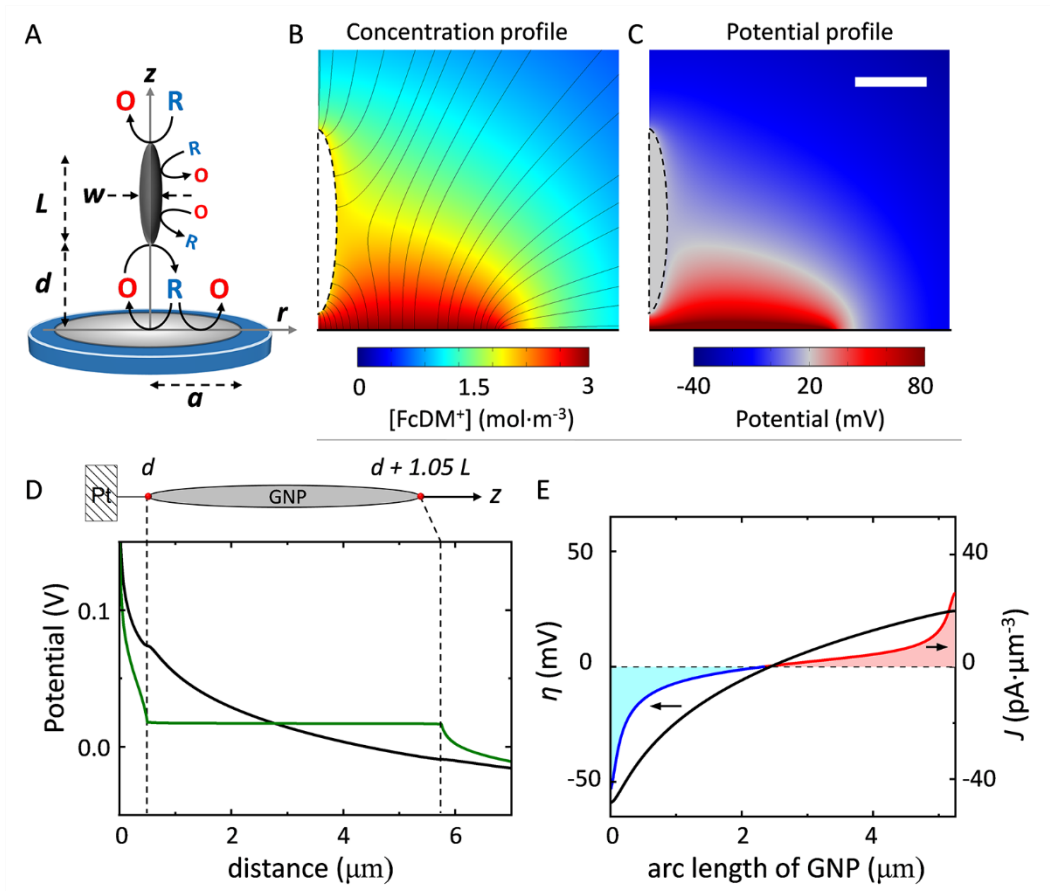
5 To explain our observation, we propose the existence of the positive feedback mechanism
 6 powered by bipolar electrochemistry, as shown in Figure 3A. The GNP behaves as a bipolar
 7 electrode. FcDM (species “R” in Figure 3A) is oxidized at the extremity of the GNP the furthest
 8 in solution while FcDM⁺ (species “O” in Figure 3A) is being reduced back to FcDM at the
 9 extremity of the GNP closest from the UME. The regenerated FcDM can diffuse to the UME and
 10 be oxidized again hence increasing the anodic current. Positive feedback has been evidenced
 11 with SECM tips approaching unbiased conducting substrates⁴²⁻⁴⁴ as well as networks of micro-
 12 ring electrodes at the bottom of a well in proximity with a high-area gold layer that is not
 13 electrically connected to the ring electrodes and left floating at the potential of the solution.^{45, 46}

14 To support our hypothesis, we performed 2D axial numerical simulations describing the
 15 oxidation of FcDM on the UME in presence of a spheroidal conducting GNP, as depicted in

1 Figure 3A. The details of the simulation are provided in supporting information. The presence of
2 a conducting GNP locally disturbs the concentration profile of FcDM^+ (see Figure 3B).
3 However, these changes are not observed in presence of an insulating analog (see Figure S10A).
4 Interestingly the concentration of FcDM^+ and FcDM remains constant (orange color) over the
5 entire surface of the GNP, and the flux of FcDM^+ increases strongly between the bottom of the
6 GNP and the UME (higher concentration of flux lines) indicating positive feedback for the UME
7 in agreement with our observation. Figure 3C presents the potential map calculated from the
8 concentration profile via the Nernst equation. The variation of $[\text{O}]/[\text{R}]$ in the diffusion layer by
9 2-3 order of magnitudes produces a difference of potential on the order of 120-180 mV near the
10 Pt surface. A fraction of this potential difference will provide the electromotive force to drive
11 faradaic reactions at both ends of the GNP in an attempt to locally reach chemical equilibrium.
12 The equilibrium is reached when the concentrations at both ends are equal. As found in our
13 simulation the potential within the GNP is constant and floats at about 17 mV (vs $E_{\text{FcDM}^+/\text{FcDM}}^0$)
14 (gray color in Figure 3C).

15 The potential along the arc length of the GNP is plotted in green in Figure 3D, while the
16 potential computed for an insulating analog is in black. The difference between both potentials
17 provides the driving force for the oxidation/reduction of $\text{FcDM}/\text{FcDM}^+$ at the surface of GNP.
18 The computed driving force (η , defined as the potential of the GNP vs $E_{\text{FcDM}^+/\text{FcDM}}^0$) for the
19 oxidation/reduction of $\text{FcDM}/\text{FcDM}^+$ at the GNP surface is plotted in Figure 3E (black trace on
20 the left axis). It follows a logarithm relationship with the position along the GNP because of the
21 non-linear concentration profile of $\text{FcDM}/\text{FcDM}^+$ in the diffusion layer of the UME.
22 Importantly, the sign of the driving force changes near the center of the GNP. As a result, both
23 anodic and cathodic currents are expected to flow on the same object, as shown in red and blue

1 traces on the right axis in Figure 3E, respectively. The integration of the anodic and cathodic
 2 current densities

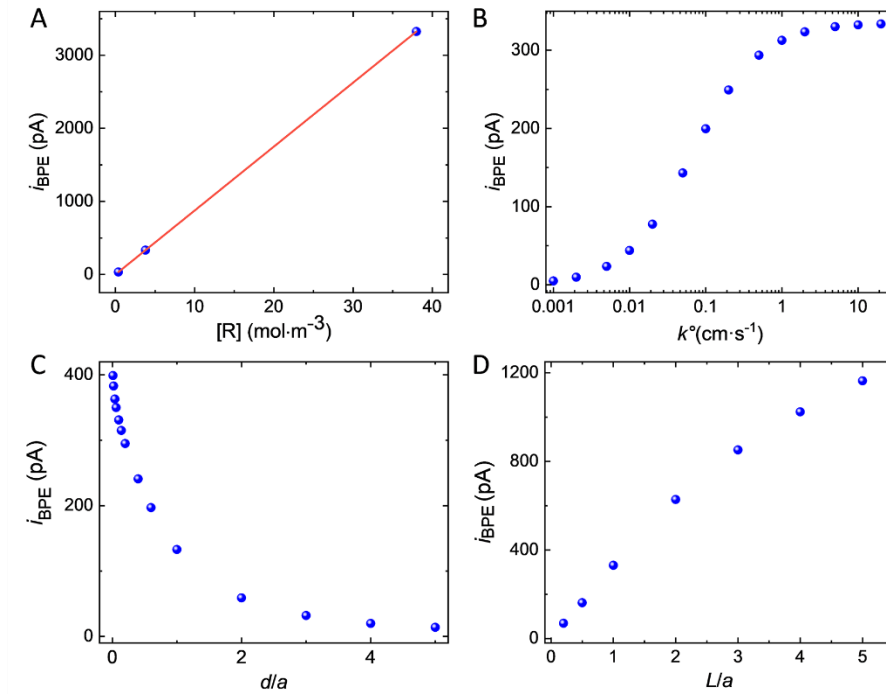


3
 4 Figure 3. (A) Schematic illustration of the bipolar feedback mechanism on a “model” spheroidal GNP of
 5 length L and width W positioned at a distance d from the UME. (B) Concentration profile of FcDM^+ near the
 6 UME at a steady state where the black lines represent the normal flux of FcDM^+ . (C) Potential profile
 7 calculated from the concentration profile in (B) via Nernst equation. The scale bar represents $2\ \mu\text{m}$. (D)
 8 Potential along the z-axis of symmetry and the arc length of the GNP (schematically shown on top). The actor
 9 1.05 comes from the difference between the length and the cord of a spheroid. The green and black traces are
 10 obtained for a conducting GNP and an insulating analog, respectively. (E) The driving force (black trace on the
 11 left axis) generated from the potential difference in (D) allows passing a current density shown on the right
 12 axis. The anodic and cathodic current densities are plotted in red and blue, respectively. The total bipolar
 13 current flowing through the GNP is 331 pA.

1 along the entire surface of the GNP leads to no net charging of the GNP (as imposed in our
2 model). The simulated bipolar current, i_{BPE} , flowing through the GNP is a function of multiple
3 experimental parameters. It depends on the concentration of the redox species, the kinetics of
4 electron transfer, the distance between the GNP and the UME, as well as the size of the GNP.
5 We computed i_{BPE} as a function of the initial concentration of [R] as well as the initial ratio
6 [O]/[R] in solution. The bipolar current is proportional to the initial concentration of [R] (see
7 Figure 4A) but independent of the initial ratio O/R (see Figure S11). In practice, it is thus
8 advantageous to maximize the current at the UME by using a high concentration of redox
9 species. The presence of the other form of the redox couple (FcDM^+ in our case) does not affect
10 the bipolar current since the driving force for bipolar electrochemistry does not depend on the
11 ratio of [O]/[R] at a certain position but the difference of [O]/[R] between two different
12 positions. On the other hand, the choice of the redox couple can drastically influence the kinetics
13 of the electron transfer and in return i_{BPE} . Figure 4B shows i_{BPE} as a function of k° . For a
14 Nernstian system (like $\text{FcDM}^+/\text{FcDM}$), i_{BPE} is limited by mass transfer. As k° decreases below
15 $0.01 \text{ cm}\cdot\text{s}^{-1}$, i_{BPE} decreases by two orders of magnitude. Electro-catalytic reactions should thus be
16 avoided or considered only when the material of the floating particle is a good catalyst. A fast
17 redox couple such as metallocene compounds is best suited.

18 We will now examine how the size and position of the GNP affect the bipolar feedback
19 current. Figure 4C shows the bipolar current as a function of the GNP-UME distance normalized
20 by the radius of the UME, denoted as d/a . The bipolar current decreases exponentially as the
21 GNP is further away from the surface of the UME. Bipolar current is on the order of hundreds of
22 pA when the GNP is closer than one electrode's radii from the surface. Figure 4D shows the
23 bipolar current as a function of the length of the GNP relative to the size of the UME, denoted as

1 L/a . The distance between the bottom of the GNP and the surface of the UME is constant (0.5
2 μm). The longer is the GNP and the higher is the bipolar current. This latter tends toward a
3 plateau when the length of the GNP equals about five times the radius of the UME. The variation
4 of driving force at the GNP explains this trend. When the GNP is small compared to the size of
5 the diffusion layer at the UME (proportional to the radius of the UME), the potential gradient
6 explored by the two extremities of the GNP is small and so is the driving force. On the other
7 hand, once the GNP explores most of the diffusion layer (95% of the concentration gradient is
8 contained within two UME's radius) no significant gain in driving force is possible.

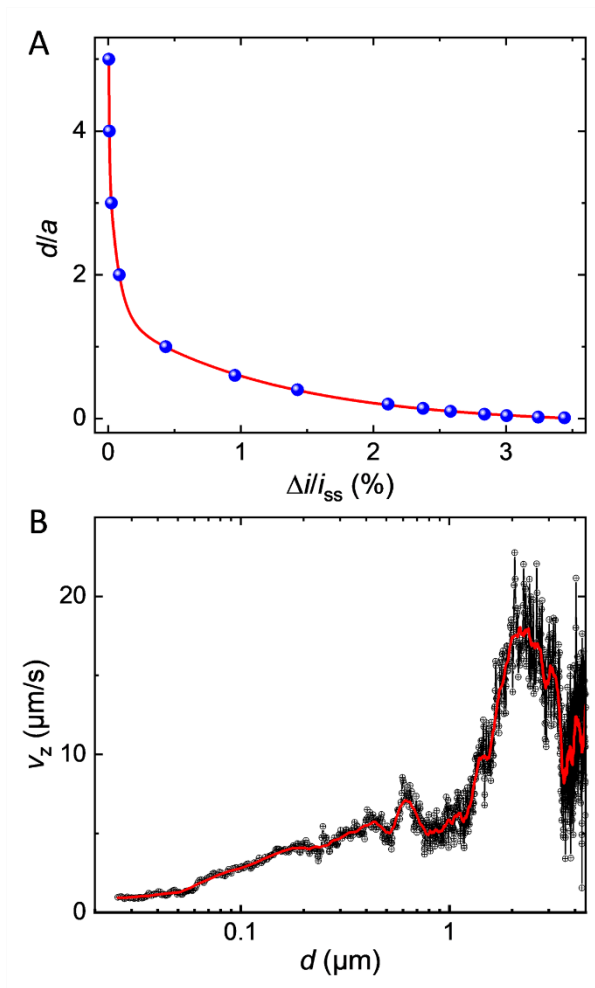


9
10 Figure 4. Simulated bipolar current, i_{BPE} , as a function of (A) the initial concentration of $[R]$ and (B) the kinetic
11 constant of k° . (C) Bipolar current simulated for $L = 5 \mu\text{m}$ tall and $1 \mu\text{m}$ large spheroidal GNP positioned at d
12 above the surface of a $a = 5 \mu\text{m}$ radius UME, and (D) Bipolar current simulated for a $L \mu\text{m}$ tall and $1 \mu\text{m}$ large
13 spheroidal GNP positioned at $d = 0.5 \mu\text{m}$ above the surface of a $a = 5 \mu\text{m}$ radius UME.

1 As a matter of fact, only a fraction of this bipolar current will lead to a positive feedback
2 current at the UME. Figure 5A shows the simulated bipolar feedback current (relative to its value
3 in absence of GNP) at various adimensional distances, d/a , from the UME. The red line is a
4 combination of exponential functions adjusted on the blue dots. As the GNP is approaching the
5 UME at less than one electrode's radius the feedback rises from 0.1% up to a couple of % at 50
6 nm from the UME. The closer the GNP the stronger is the feedback current. This trend is caused
7 by two phenomena. First, as the GNP is further away in solution the bipolar current decreases
8 (see Figure 4C). Indeed, the driving force drops as the concentration gradient fades away in
9 solution. Second, as the GNP is further away in solution the collection efficiency decreases (see
10 Figure S12).

11 We used the red line as a simulated approach curve to deduce the distance between the GNP
12 and the UME at every time during the chronoamperogram shown in Figure 1C (red part) and
13 then, calculated the derivative with respect to time to obtain the instantaneous velocity of the
14 GNP along the direction normal to the surface (V_z). The velocity V_z is plotted in Figure 5B in
15 black as a function of d (on a log scale). At several μm from the surface of the electrode, the
16 GNP seems to accelerate and then, at $d = 2 \mu\text{m}$ decelerate from 15-20 $\mu\text{m/s}$ to few $\mu\text{m/s}$. Another
17 velocity profile obtained for a different GNP is provided in Figure S13, and the simultaneous
18 movie is provided in Movie S2. While the uncertainty on the measurement is large far from the
19 UME, the process of deceleration benefits from the high sensitivity of positive feedback at short
20 distances. A deceleration indicates that the resulting forces acting on the GNP are not constant.
21 Recent works showed that electro-osmotic flow (EOF) should dominate the mass transport of
22 particles under our low supporting electrolyte condition.^{33, 34} The simulated velocity profile of

- 1 EOF presents a decrease of tangential velocity when the liquid coming from above the electrode
- 2 turns just above the surface in agreement with our observations.



3
 4 Figure 5. (A) Simulated bipolar feedback current (blue dots) versus normalized distance between the UME and
 5 the GNP. The red line results from the adjustments of the function $Y(x) = -0.43 + 7.66 e^{-x/1.23} + 17.8 e^{-x/0.005} +$
 6 $11.1 e^{-x/0.07}$, $R^2 = 0.9998$. (B) Velocity profile of the GNP obtained by calculating the time-derivative of the
 7 GNP-UME distance found from the simulated approach curve in (A). The red line is smooth of the black
 8 points (adjacent-averaging window 205 points, reflect boundary).

9 Conclusions

10 In conclusion, we evidenced micro/nano-scale interactions between individual GNPs and an
 11 electrified surface. We developed a new technique to monitor the interaction dynamics, in a

1 contact-less mode, of GNPs few μm down to few tens of nm from a Pt disk with a high temporal
2 resolution at the millisecond timescale. We explain, based on numerical simulations, the key
3 parameters affecting the magnitude and shape of the current transient. A quantitative relationship
4 between the position of the GNP and the current transient was established allowing us to
5 estimate the velocity of GNPs at extremely short distances from the surface. We found the GNP
6 experienced a strong deceleration from few tens of $\mu\text{m/s}$ down to few $\mu\text{m/s}$ within the last μm
7 above the surface, indicating the existence of highly inhomogeneous micron-range forces near
8 the surface.

9 This technique potentially enables the electrochemical study of nanoscale dynamics of any
10 micro/nano-particles with a large aspect ratio near an electrified surface in which gradients of
11 electric potential or chemical potential exist between particles and electrified surfaces. Those
12 particles, to name but a few, could potentially be graphene nanosheet, carbon nanotube, thin
13 metal chalcogenides (i.e. MoS_2 , WS_2 , and PtS_2),⁴⁷ and Mxenes (i.e. Ti_2AlC , Ti_3AlC_2 , and
14 Ta_4AlC_3).⁴⁸

15 **Methods**

16 **Chemicals.** 1,1'-ferrocenedimethanol (FcDM), Sodium hydroxide, poly(4-styrene sulfonic acid)
17 (PSS), and poly(allylamine hydrochloride) (PAA) were purchased from Sigma-Aldrich and used
18 without further purification. DI-water ($18.2 \text{ M}\Omega\cdot\text{cm}$) was produced with an Elix Milli-Q water
19 station (Millipore).

20 **Graphene nanoplatelet suspension.** The suspension of GNPs was prepared by mixing 10 mg of
21 GNP powder in 100 mL of a 0.01% v/v PSS solution, sonicating for 30 min, and then
22 centrifugation. The first centrifugation of 1 min at 11000 g was used to remove the large GNPs.
23 Only the supernatant was kept. The two following centrifugations were performed 10 min at

1 5000 g and the supernatant was discarded to remove the small fragments of GNP. The GNP
2 suspension was sonicated 5 min between each centrifugation to help re-dispersing the GNPs. The
3 concentration of GNP used in this work was measured by UV-Visible adsorption (Cary 50 Scan,
4 Variant). The details are provided in Figure S1.

5 **Electrode fabrication.** Pt ultramicroelectrode (inlaid disk) was fabricated by heat sealing a 10
6 μm Pt wire (Goodfellow, hard temper) in a borosilicate glass capillary (2 mm o.d., 1.16 mm i.d.)
7 using a heating coil. The side of the wire is exposed by polishing the capillary with sandpaper
8 and then alumina slurry (down to 0.1 μm , Buehler) until obtaining a mirror-like surface. The
9 ultra-microelectrode (UME) is sharpened by manually polishing the side of the capillary on
10 sandpaper until achieving an RG = 15 (see Figure S2).

11 **Opto-electrochemical setup.** The opto-electrochemical setup consists of an inverted microscope
12 (ix73, Olympus, 40X objective) and a correlated electrochemical setup housed in a Faraday cage.
13 A two-electrode setup is used to measure the current and apply a potential versus an Ag/AgCl
14 3.4 M KCl reference electrode. The cell is placed onto an inverted microscope to acquire bright-
15 field videos in reflectance. The camera and the ammeter are synchronized externally and data is
16 collected at 1 kHz and 2 kHz, respectively. Additional experimental details about the apparatus
17 are provided in Figure S6.

18 **Numerical Simulation.** The simulations were performed with COMSOL Multiphysics 5.3a in
19 2D axial geometry with the stationary solution. The diffusion of FcDM molecules is governed by
20 Fick's law (Transport of diluted species module), the potential inside the GNP is governed by
21 Ohm's law (Electric Currents module), and the electron transfer kinetics at the surface of the
22 UME and GNP is governed by Butler-Volmer equation. The bipolar current passing through
23 GNP and the current at the Pt electrode is simulated by integrating the total normal flux to the

1 GNP surface and the electrode surface under steady-state simulation conditions, respectively.
2 The details are provided in the supporting information.

3 **ASSOCIATED CONTENT**

4 **Supporting Information**

5 The Supporting Information is available free of charge.

6 The supporting information contains two videos (Video S1 and Video S2) and twelve sections:
7 (I) The chemicals and materials; (II) Electrode fabrication; (III) SEM characterization of GNPs;
8 (IV) Image analysis; (V) Opto-electrochemical setup; (VI) blank measurement; (VII) effect of
9 the viscosity on the velocity of GNP; (VIII) Numerical Simulations; (IX) Simulated
10 concentration and potential profiles near UME; (X) collection efficiency; (XI) The velocity of
11 GNP approaching the UME; (XII) Reference.

12 **AUTHOR INFORMATION**

13 **Corresponding Author**

14 * **Christophe Renault:**

15 <https://orcid.org/0000-0003-4525-8702>; E-mail: christophe.renault@polytechnique.edu

16 **Authors**

17 **Present Addresses**

18 **Zejun Deng:**

19 † Institute for Health Innovation & Technology, National University of Singapore, Singapore
20 117599, Singapore; <https://orcid.org/0000-0002-4069-6896>

21 **Author Contributions**

1 All authors performed experiments, built finite element simulations, and collected/processed
2 data. The manuscript was written through the contributions of all authors. All authors have
3 approved the final version of the manuscript.

4 **Funding Sources**

5 This work is support by the CNRS, the Agence Nationale de la Recherche (ANR-17-CE09-0034-
6 01, “SEE”) and the China Scholarship Council (201706370055). We thank “Institute for Health
7 Innovation & Technology” at NUS for permitting us to use the simulation workstation.

8 **Notes**

9 The authors declare no competing financial interest.

10 **ACKNOWLEDGMENT**

11 This work is support by the CNRS, the Agence Nationale de la Recherche (ANR-17-CE09-0034-
12 01, “SEE”) and the China Scholarship Council (201706370055). We thank “Institute for Health
13 Innovation & Technology” at NUS for permitting us to use the simulation workstation.

14 **REFERENCES**

- 15 1. Nel, A. E.; Mädler, L.; Velegol, D.; Xia, T.; Hoek, E. M.; Somasundaran, P.; Klaessig, F.; Castranova,
16 V.; Thompson, M., Understanding biophysicochemical interactions at the nano–bio interface. *Nat. Mater.*
17 **2009**, *8* (7), 543-557.
- 18 2. Wu, C.-Y.; Wolf, W. J.; Levartovsky, Y.; Bechtel, H. A.; Martin, M. C.; Toste, F. D.; Gross, E., High-
19 spatial-resolution mapping of catalytic reactions on single particles. *Nature* **2017**, *541* (7638), 511-515.
- 20 3. Limo, M. J.; Sola-Rabada, A.; Boix, E.; Thota, V.; Westcott, Z. C.; Puddu, V.; Perry, C. C., Interactions
21 between metal oxides and biomolecules: from fundamental understanding to applications. *Chem. Rev.*
22 **2018**, *118* (22), 11118-11193.

- 1 4. Lemineur, J. F.; Noël, J. M.; Ausserré, D.; Combellas, C.; Kanoufi, F., Combining Electrodeposition and
2 Optical Microscopy for Probing Size- Dependent Single- Nanoparticle Electrochemistry. *Angew. Chem.*
3 *Int. Ed.* **2018**, *57* (37), 11998-12002.
- 4 5. Ma, H.; Chen, J. F.; Wang, H. F.; Hu, P. J.; Ma, W.; Long, Y. T., Exploring dynamic interactions of
5 single nanoparticles at interfaces for surface-confined electrochemical behavior and size measurement.
6 *Nat. Commun.* **2020**, *11* (1), 2307.
- 7 6. Nicolai, L.; Schiefelbein, K.; Lipsky, S.; Leunig, A.; Hoffknecht, M.; Pekayvaz, K.; Raude, B.; Marx, C.;
8 Ehrlich, A.; Pircher, J., Vascular surveillance by haptotactic blood platelets in inflammation and infection.
9 *Nat. Commun.* **2020**, *11* (1), 1-16.
- 10 7. Xiao, X., Bard, Allen J, Observing single nanoparticle collisions at an ultramicroelectrode by
11 electrocatalytic amplification. *J. Am. Chem. Soc.* **2007**, *129* (31), 9610-9612.
- 12 8. Xiao, X.; Fan, F.-R. F.; Zhou, J.; Bard, A. J., Current transients in single nanoparticle collision events. *J.*
13 *Am. Chem. Soc.* **2008**, *130* (49), 16669-16677.
- 14 9. Zhou, Y. G.; Rees, N. V.; Compton, R. G., The electrochemical detection and characterization of silver
15 nanoparticles in aqueous solution. *Angew. Chem. Int. Ed.* **2011**, *50* (18), 4219-21.
- 16 10. Brasiliense, V.; Berto, P.; Combellas, C.; Tessier, G.; Kanoufi, F. d. r., Electrochemistry of single
17 nanodomains revealed by three-dimensional holographic microscopy. *Acc. Chem. Res.* **2016**, *49* (9),
18 2049-2057.
- 19 11. Baker, L. A., Perspective and Prospectus on Single-Entity Electrochemistry. *J. Am. Chem. Soc.* **2018**, *140*
20 (46), 15549-15559.
- 21 12. Wang, W., Imaging the chemical activity of single nanoparticles with optical microscopy. *Chem. Soc.*
22 *Rev.* **2018**, *47* (7), 2485-2508.
- 23 13. Xiang, Z. p.; Deng, H. q.; Peljo, P.; Fu, Z. y.; Wang, S. l.; Mandler, D.; Sun, G. q.; Liang, Z. x.,
24 Electrochemical dynamics of a single platinum nanoparticle collision event for the hydrogen evolution
25 reaction. *Angew. Chem. Int. Ed.* **2018**, *130* (13), 3522-3526.

- 1 14. Evers, M. V.; Bernal, M.; Roldan Cuenya, B.; Tschulik, K., Piece by Piece—Electrochemical Synthesis
2 of Individual Nanoparticles and their Performance in ORR Electrocatalysis. *Angew. Chem. Int. Ed.* **2019**,
3 58 (24), 8221-8225.
- 4 15. Zhou, M.; Bao, S.; Bard, A. J., Probing size and substrate effects on the hydrogen evolution reaction by
5 single isolated Pt atoms, atomic clusters, and nanoparticles. *J. Am. Chem. Soc.* **2019**, *141* (18), 7327-
6 7332.
- 7 16. Jin, Z.; Bard, A. J., Atom-by-atom electrodeposition of single isolated cobalt oxide molecules and clusters
8 for studying the oxygen evolution reaction. *Proc. Natl. Acad. Sci.* **2020**, *117* (23), 12651-12656.
- 9 17. Choo, P.; Liu, T.; Odom, T. W., Nanoparticle Shape Determines Dynamics of Targeting Nanoconstructs
10 on Cell Membranes. *J. Am. Chem. Soc.* **2021**, *143*, 4550-4555.
- 11 18. Brasiliense, V.; Patel, A. N.; Martinez-Marrades, A.; Shi, J.; Chen, Y.; Combellas, C.; Tessier, G.;
12 Kanoufi, F., Correlated Electrochemical and Optical Detection Reveals the Chemical Reactivity of
13 Individual Silver Nanoparticles. *J. Am. Chem. Soc.* **2016**, *138* (10), 3478-83.
- 14 19. Hao, R.; Fan, Y.; Zhang, B., Imaging Dynamic Collision and Oxidation of Single Silver Nanoparticles at
15 the Electrode/Solution Interface. *J. Am. Chem. Soc.* **2017**, *139* (35), 12274-12282.
- 16 20. Ma, W.; Ma, H.; Chen, J. F.; Peng, Y. Y.; Yang, Z. Y.; Wang, H. F.; Ying, Y. L.; Tian, H.; Long, Y. T.,
17 Tracking motion trajectories of individual nanoparticles using time-resolved current traces. *Chem. Sci.*
18 **2017**, *8* (3), 1854-1861.
- 19 21. Oja, S. M.; Robinson, D. A.; Vitti, N. J.; Edwards, M. A.; Liu, Y.; White, H. S.; Zhang, B., Observation
20 of Multipeak Collision Behavior during the Electro-Oxidation of Single Ag Nanoparticles. *J. Am. Chem.*
21 *Soc.* **2017**, *139* (2), 708-718.
- 22 22. Robinson, D. A.; Liu, Y.; Edwards, M. A.; Vitti, N. J.; Oja, S. M.; Zhang, B.; White, H. S., Collision
23 Dynamics during the Electrooxidation of Individual Silver Nanoparticles. *J. Am. Chem. Soc.* **2017**, *139*
24 (46), 16923-16931.
- 25 23. Ustarroz, J.; Kang, M.; Bullions, E.; Unwin, P. R., Impact and oxidation of single silver nanoparticles at
26 electrode surfaces: one shot versus multiple events. *Chem. Sci.* **2017**, *8* (3), 1841-1853.

- 1 24. Li, S.; Du, Y.; He, T.; Shen, Y.; Bai, C.; Ning, F.; Hu, X.; Wang, W.; Xi, S.; Zhou, X., Nanobubbles: An
2 effective way to study gas-generating catalysis on a single nanoparticle. *J. Am. Chem. Soc.* **2017**, *139*
3 (40), 14277-14284.
- 4 25. German, S. R.; Edwards, M. A.; Ren, H.; White, H. S., Critical nuclei size, rate, and activation energy of
5 H₂ gas nucleation. *J. Am. Chem. Soc.* **2018**, *140* (11), 4047-4053.
- 6 26. Lemineur, J. F.; Noel, J. M.; Ausserre, D.; Combellas, C.; Kanoufi, F., Combining Electrodeposition and
7 Optical Microscopy for Probing Size-Dependent Single-Nanoparticle Electrochemistry. *Angew. Chem.*
8 *Int. Ed.* **2018**, *57* (37), 11998-12002.
- 9 27. Chen, Q.; Liu, Y.; Edwards, M. A.; Liu, Y.; White, H. S., Nitrogen Bubbles at Pt Nanoelectrodes in a
10 Nonaqueous Medium: Oscillating Behavior and Geometry of Critical Nuclei. *Anal. Chem.* **2020**, *92* (9),
11 6408-6414.
- 12 28. Gao, R.; Edwards, M. A.; Qiu, Y.; Barman, K.; White, H. S., Visualization of hydrogen evolution at
13 individual platinum nanoparticles at a buried interface. *J. Am. Chem. Soc.* **2020**, *142* (19), 8890-8896.
- 14 29. Noel, J. M.; Miranda Vieira, M.; Brasiliense, V.; Lemineur, J. F.; Combellas, C.; Kanoufi, F., Effect of
15 the driving force on nanoparticles growth and shape: an opto-electrochemical study. *Nanoscale* **2020**, *12*
16 (5), 3227-3235.
- 17 30. Lemineur, J. F.; Ciocci, P.; Noel, J. M.; Ge, H.; Combellas, C.; Kanoufi, F., Imaging and Quantifying the
18 Formation of Single Nanobubbles at Single Platinum Nanoparticles during the Hydrogen Evolution
19 Reaction. *ACS nano* **2021**, *15* (2), 2643-2653.
- 20 31. Fosdick, S. E.; Anderson, M. J.; Nettleton, E. G.; Crooks, R. M., Correlated electrochemical and optical
21 tracking of discrete collision events. *J. Am. Chem. Soc.* **2013**, *135* (16), 5994-5997.
- 22 32. Lemineur, J. F.; Noel, J. M.; Courty, A.; Ausserre, D.; Combellas, C.; Kanoufi, F., In Situ Optical
23 Monitoring of the Electrochemical Conversion of Dielectric Nanoparticles: From Multistep Charge
24 Injection to Nanoparticle Motion. *J. Am. Chem. Soc.* **2020**, *142* (17), 7937-7946.
- 25 33. Moazzenzade, T.; Yang, X.; Walterbos, L.; Huskens, J.; Renault, C.; Lemay, S. G., Self-Induced
26 Convection at Microelectrodes via Electroosmosis and Its Influence on Impact Electrochemistry. *J. Am.*
27 *Chem. Soc.* **2020**, *142* (42), 17908-17912.

- 1 34. Thorgaard, S. N.; Jenkins, S.; Tarach, A. R., Influence of Electroosmotic Flow on Stochastic Collisions at
2 Ultramicroelectrodes. *Anal. Chem.* **2020**, *92* (18), 12663-12669.
- 3 35. Pendergast, A. D.; Deng, Z.; Maroun, F.; Renault, C.; Dick, J. E., Revealing Dynamic Rotation of Single
4 Graphene Nanoplatelets on Electrified Microinterfaces. *ACS Nano* **2021**, *15* (1), 1250-1258.
- 5 36. Robinson, D. A.; Edwards, M. A.; Liu, Y.; Ren, H.; White, H. S., Effect of Viscosity on the Collision
6 Dynamics and Oxidation of Individual Ag Nanoparticles. *J. Phys. Chem. C* **2020**, *124* (16), 9068-9076.
- 7 37. Sun, L.; Wang, W.; Chen, H. Y., Dynamic Nanoparticle- Substrate Contacts Regulate Multi- Peak
8 Behavior of Single Silver Nanoparticle Collisions. *ChemElectroChem* **2018**, *5* (20), 2995-2999.
- 9 38. Chen, H. B.; Jiang, D.; Zhou, X. L.; Qian, C.; Yang, Y.; Liu, X. W., Tracking Interfacial Dynamics of a
10 Single Nanoparticle Using Plasmonic Scattering Interferometry. *Anal. Chem.* **2020**, *92* (19), 13327-
11 13335.
- 12 39. Wonner, K.; Evers, M. V.; Tschulik, K., Simultaneous Opto- and Spectro-Electrochemistry: Reactions of
13 Individual Nanoparticles Uncovered by Dark-Field Microscopy. *J. Am. Chem. Soc.* **2018**, *140* (40),
14 12658-12661.
- 15 40. Sundaresan, V.; Monaghan, J. W.; Willets, K. A., Visualizing the effect of partial oxide formation on
16 single silver nanoparticle electrodisolution. *J. Phys. Chem. C* **2018**, *122* (5), 3138-3145.
- 17 41. Noël, J.-M.; Lemineur, J.-F., Optical microscopy to study single nanoparticles electrochemistry: from
18 reaction to motion. *Curr. Opin. Electrochem.* **2020**, 100647.
- 19 42. Xiong, H.; Guo, J.; Amemiya, S., Probing heterogeneous electron transfer at an unbiased conductor by
20 scanning electrochemical microscopy in the feedback mode. *Anal. Chem.* **2007**, *79* (7), 2735-2744.
- 21 43. Oleinick, A. I.; Battistel, D.; Daniele, S.; Svir, I.; Amatore, C., Simple and clear evidence for positive
22 feedback limitation by bipolar behavior during scanning electrochemical microscopy of unbiased
23 conductors. *Anal. Chem.* **2011**, *83* (12), 4887-93.
- 24 44. Sun, T.; Wang, D.; Mirkin, M. V., Electrochemistry at a single nanoparticle: from bipolar regime to
25 tunnelling. *Faraday Discuss.* **2018**, *210* (0), 173-188.
- 26 45. Oleinick, A.; Yan, J.; Mao, B.; Svir, I.; Amatore, C., Theory of microwell arrays performing as
27 generators–collectors based on a single bipolar plane electrode. *ChemElectroChem* **2016**, *3* (3), 487-494.

- 1 46. He, D.; Yan, J.; Zhu, F.; Zhou, Y.; Mao, B.; Oleinick, A.; Svir, I.; Amatore, C., Enhancing the Bipolar
2 Redox Cycling Efficiency of Plane-Recessed Microelectrode Arrays by Adding a Chemically Irreversible
3 Interferent. *Anal. Chem.* **2016**, 88 (17), 8535-8541.
- 4 47. Zhou, J.; Lin, J.; Huang, X.; Zhou, Y.; Chen, Y.; Xia, J.; Wang, H.; Xie, Y.; Yu, H.; Lei, J., A library of
5 atomically thin metal chalcogenides. *Nature* **2018**, 556 (7701), 355-359.
- 6 48. Naguib, M.; Mochalin, V. N.; Barsoum, M. W.; Gogotsi, Y., 25th anniversary article: MXenes: a new
7 family of two- dimensional materials. *Adv. Mater.* **2014**, 26 (7), 992-1005.

8

Table of Contents

